Journal of Sustainable Development of Smart Energy Networks

https://www.sdewes.org/jsdsen

Year 2026, Volume 1, Issue 3, 2030707

Original Research Article

Preliminary Energy and Economic Assessment of a Photovoltaic-Driven Heat Pump System for a Thermal Prosumer in the Southern Mediterranean Region

Pietro Catrini, Stefania Guarino, Maurizio La Villetta, Antonio Piacentino
Department of Engineering, University of Palermo, Viale delle Scienze Building no. 9, Palermo, Italy
e-mail: pietro.catrini@unipa.it, stefania.guarino@unipa.it, maurizio.lavilletta@unipa.it, antonio.piacentino@unipa.it

Cite as: Catrini, P., Guarino, S., La Villetta, M., Piacentino, A., Preliminary Energy and Economic Assessment of a Photovoltaic-Driven Heat Pump System for a Thermal Prosumer in the Southern Mediterranean Region, J. sustain. dev. smart. en. net., 1(3), 2030707, 2026, DOI: https://doi.org/10.13044/j.sdsen.d3.0707

ABSTRACT

District heating and cooling networks can support renewable energy source integration by converting surplus electricity through distributed power-to-heat & cold technologies. In this respect, end-users will be active participants (i.e., prosumers) capable of both consuming and producing heat or cold, which is eventually sold to the district network. This study presents an integrated energy and economic assessment of a photovoltaic-driven air-to-water heat pump system operating as a thermal prosumer in a Mediterranean office building connected to a district heating and cooling network. Building energy demand is simulated in TRNSYS, heat pump performance is modelled using IMST-ART, and PV generation is evaluated through a Python-based optimization framework. Annual results show a photovoltaic generation of 363 MWh, with 60.7% self-consumption and 39.3% surplus. In the thermal prosumer configuration, 47.03 MWh y^{-1} of heat and 168.52 MWh y^{-1} of cooling are supplied to the network, while 72.19 MWh y^{-1} of electricity is exported to the grid. Economic analysis indicates that exporting electricity yields an internal rate of return of 16.2%, whereas the thermal prosumer scenario achieves an internal rate of return of 11.9%, increasing to 15.5% when heat and cold are sold at 11 c€ kWh^{-1}. Results highlight the strong dependence of profitability on thermal energy remuneration. Finally, the study shows the potential of photovoltaic-driven heat pump integration with district heating and cooling networks in Mediterranean contexts, provided that adequate market mechanisms are in place to valorize thermal energy.

KEYWORDS

District Heating and Cooling, Space Heating and Cooling, Photovoltaic, Heat Pump, Thermal Prosumer, Energy Efficiency.

INTRODUCTION

District heating and cooling networks (DHCN) are key infrastructures for the transition towards low-carbon and renewable energy systems [1]. In this respect, they facilitate large-scale integration of renewable energy sources (RES) [2] and provide an effective means for exploiting low-temperature waste heat from industries [3] and data centres [4]. Meantime, they enable energy networks coupling thanks to power-to-heat & cold technologies [5], converting surplus electricity and mitigating the variability of solar and wind generation. [6].

Like electric smart grids, the role of prosumers will be central in future DHCNs [7]. In this scenario, end-users are no longer passive nodes, but active participants capable of both

consuming and producing thermal energy [8], thereby contributing to the flexibility of the overall system [9]. For this reason, recent studies on DHCNs focused on proposing novel substation configurations for a bidirectional heat exchange[10], on re-design [11] and modelling [12] of the entire network with the presence of prosumers and developing innovative trading schemes to promote heat/cold sharing [13].

Within this framework, solar energy systems, such as photovoltaic (PV)-driven heat pumps (HP) and solar thermal technologies, represent key enablers for the transition of end-users into prosumers [14]. Consequently, an increasing part of research has addressed the integration and operation of solar prosumers in DHCNs, focusing on diverse yet complementary aspects.

Some authors have proposed methods to forecast surplus heat from solar systems, available for sharing within DHCNs. In this respect, Ricci et al. [15] proposed an innovative model based on artificial neural networks to forecast heat generation from a solar-based prosumer, relying on meteorological data and historical measurements. Other authors have developed novel substation layouts to enable bidirectional heat exchange between users and DHCNs, assuming solar energy technologies as on-site heat generation units. For example, Sdringola et al. [16] confirmed that bidirectional substations can enhance solar heat self-consumption through optimized storage management, temperature control, and HP integration. Zinsmeister et al. [17] compared different configurations for a prosumer substation, showing that layouts integrating solar thermal collectors or PV-driven HPs with local thermal storage can increase on-site heat utilization by up to 20-30%. Dino et al. [18] performed a techno-economic analysis of a high-vacuum solar thermal system integrated into a prosumer's substation, while mapping the impact of heat selling economic revenues from. Gianaroli et al. [19] propose a non-invasive retrofit of a substation to enable thermal prosumer operation and solar heat recovery in existing networks in Northern Italy, achieving 78.4% solar energy utilization.

Other studies focused on the effects of network design and topology on the utilization of distributed solar energy plants. Liu et al. [20] addressed the joint optimization of district network layout and pipe diameters with distributed solar plants. Using a mixed-integer optimization routine, results show that the proposed method can reduce total investment and operating costs by about 10-25% compared to conventional design approaches. Akbar and Kilkis[21] proposed an exergy-based optimization routine for PV-thermal prosumers, including onboard green hydrogen production. The model introduced exergy constraints to optimally balance electrical, thermal, and chemical energy flows, showing primary energy savings up to 25-35% compared to energy-based optimization approaches.

Other studies focused on energy, economic, and environmental benefits from including solar prosumers in DHCNs. Bogdanovics et al. [22] investigated a small-scale district heating system used as thermal storage for decentralized solar thermal collectors during the non-heating period. Results showed that the network can absorb and store up to 60-80% of excess solar thermal production, significantly reducing solar curtailment and improving seasonal utilization. Lee et al. [23] analysed heat trading between two large-scale prosumers equipped with solar and ground energy systems connected to a DHCN. Results showed that bilateral heat trading enables cost savings up to 16-25% and primary energy reductions of about 10-20% compared to independent operation of the prosumers. Calise et al. [24] investigated a solar-driven 5th-generation DHCNs with ground-source HPs for a 50-building district in Leganés (Madrid). Their thermo-economic analysis showed a primary energy savings index of about 64% and a carbon dioxide (CO_2) emissions reduction of approximately 76% compared to the reference case, although the system's economic payback period was relatively long (~33 years) due to high installation cost. Tang et al. [25] developed a dynamic and techno-economic model of a distributed solar heating system coupled with a busbar-based thermal reservoir network. Simulation results showed that the proposed architecture increases solar thermal utilization by 20-35% and reduces auxiliary energy consumption by 15-25% compared to conventional decentralized storage solutions. Frison et al. [26] investigated model predictive control strategies for bidirectional heat transfer in a prosumer substation with solar systems. Results

demonstrated that a 10-30% reduction in peak heat exchange could be achieved compared to rule-based control strategies, with an increase in solar energy utilization by up to 25%. Testasecca et al. [27] presented an energy assessment of solar-powered DHCNs serving a cluster of buildings in a Mediterranean climate. Simulation results show that solar thermal integration can cover 40-60% of annual heating demand and up to 70% of cooling demand, significantly reducing reliance on conventional energy sources. Russo et al. [28] presented a techno-economic analysis of solar energy integration in a low-temperature network, considering multiple solar technologies and system layouts. Results showed that solar integration can cover 30-70% of annual thermal demand, leading to CO_2 emission reductions up to 40-60% and system cost reductions of 10-35%, depending on technology mix and network temperature levels. Zeng et al. [29] investigated next-generation zero-carbon heating plants integrating solar thermal, PV systems, and thermal energy storage. Results show that the proposed configurations can achieve RES shares above 80-90%, with CO_2 emission reductions exceeding 85% compared to conventional fossil-based heating plants. Zajacs et al.[30] analysed the integration of decentralized solar thermal collectors connected at the substation level in a DHCNs, showing that distributed solar systems operating at supply temperatures of 60-70 °C can cover up to 20-30% of the annual heat demand and reduce both peak loads and return temperatures in the network.

Finally, a large share of recent studies has focused on the benefits arising from the integration of PV systems and HPs, also considering their impacts on the power grid, such as avoided curtailment, and their interaction with DHCNs through seasonal energy storage. For instance, Pans et al. [31] investigated low-carbon district heating configurations integrating HPs powered by RES electricity sources (including on-site PV generation) together with seasonal thermal energy storage, demonstrating that optimized system designs can achieve CO_2 emission reductions of up to approximately 98%. Somawanshi et al. [32] analysed the optimal scheduling of smart HPs integrated with PV and thermal storage for a residential building. The results show that coordinated control strategies can increase RES utilization and reduce grid energy exchange by about 15–25%, improving system flexibility and load management. Kayayan et al. [33] analysed the interaction between PV electricity generation and electrified heating based on HPs in a residential energy community. Their results show that coupling HPs with PV systems can increase local RES electricity self-consumption by about 8%, although seasonal mismatches between PV production and winter heating demand remain significant. Li et al. [34] investigated the synergistic integration of electric HPs and pit thermal energy storage to enhance renewable energy utilization and CO_2 emissions reduction. Their results show that a 94,985 m^3 storage can reduce RES curtailment by 32.43% and auxiliary heating electricity consumption by 94.5%, while lowering solar collector investment by up to 56%. Liao et al. [35]developed a multi-objective optimization framework to assess heating electrification strategies in buildings integrating PV systems, HPs, and battery storage under a prosumer paradigm. Their results indicate that properly sized PV–HP systems can reduce building-related emissions by more than 50%, with potential reductions approaching 90% under optimized configurations. Sornek et al. [36] reviewed the integration of power-to-heat technologies and seasonal thermal energy storage to enhance RES utilization in heating systems. The study highlights that HPs can reach Coefficient of Performance values of 2.4–5.8, while electric boilers achieve 95–99% electricity-to-heat conversion efficiency, supporting the role of electrified heating in low-carbon energy systems. Dogkas et al. [37] analysed a hybrid heating system combining district heating, air-to-water HPs, and PV systems in a multi-apartment building using dynamic simulations. Results show that prioritizing HPs can reduce annual operating costs to 2,627 €, compared to 4,348 € with DH priority and 6,312 € with district heating only. Calise et al. [38] investigated a 5th-generation DHCN integrating a 6.29 MW PV plant, lithium-ion battery storage, and distributed HPs, showing that renewable electricity can be effectively converted into thermal energy through power-to-heat systems to meet overall heating and cooling demands. Kayayan et al. [39] analysed district-scale

configurations combining PV generation with either district heating or HPs, showing that HPs can reduce total energy demand but nearly double peak electricity import (from ~1.45 MW to ~2.87 MW), thus highlighting potential limitations in grid flexibility and peak load management. Massulli et al. [40] examined a low-temperature network powered by centralized HPs and PV generation for a cluster of 200 dwellings in Rome, showing that the CO_2 emissions are significantly reduced compared with natural-gas boilers, although achieving economic competitiveness required reductions in electricity prices and network investment costs.

Addressed the knowledge gaps and contributions of this study

From the literature reviewed above, it emerges that, despite the growing number of studies, comprehensive energy and economic analyses of solar-based prosumers in Mediterranean climates remain scarce [15,16,19,27,28]. In particular, existing works have largely overlooked the valorisation of surplus PV electricity through its conversion into both heating and cooling energy within a thermal prosumer framework. Moreover, the economic viability of such configurations under different pricing schemes—accounting for both electricity and thermal energy markets—has not been systematically investigated. Most existing research has predominantly focused on heating-dominated conditions, resulting in operational and economic assessments that differ significantly from those encountered in Southern European contexts [11,20,23]. In contrast, Mediterranean regions present specific challenges and opportunities, including high cooling loads during the summer season and abundant solar irradiance throughout the year [41]. In addition, another part of literature [32-40] has investigated the benefits of integrating HPs with PV systems, in some cases also considering their integration with district networks via seasonal storages. However, these studies typically frame the prosumer role only from an electrical perspective, focusing on electricity exchange with the grid, while neglecting the potential of prosumers to interact with thermal networks.

In the transition to a decarbonized society, the combination of building-integrated PV systems and reversible HPs connected to DHCN could represent a promising solution for enhancing power system flexibility[42] and reducing RES curtailment [6]. Then, the valorisation of surplus PV electricity through its conversion into both heat and cooling and exchange with DCHNs, particularly under realistic operating conditions and market frameworks, warrants further investigation. Addressing these gaps requires integrated modelling approaches capable of simultaneously capturing building energy demand, dynamic HP performance, and high-resolution PV generation. Such approaches are still rarely applied in a unified manner within Mediterranean contexts, limiting the ability to fully assess the techno-economic potential of thermal prosumers in these regions [24].

To address these gaps, this study presents an integrated energy and economic analysis of a renewable-based thermal prosumer connected to a district heating and cooling network in a Mediterranean context. An office building located in Palermo, Southern Italy, equipped with a PV-driven air-to-water HP, is analyzed as a case study. The proposed methodology combines detailed building energy demand modelling carried out in TRaNsient SYstem Simulation (TRNSYS) software [43], dynamic HP performance characterization using IMST-ART, and a high-resolution PV generation model developed in Python. Annual simulations are carried out to assess system performance and economic profitability coming from the valorisation of surplus PV electricity - after meeting the building's air conditioning and electrical loads - through its conversion into heat or cold via a dedicated HP and subsequent supply to the local DHCN. Specifically, the main novelties of this work can be summarized as follows:

- The study adopts an integrated multi-domain modelling framework that combines detailed building energy simulation, dynamic HP modelling, and high-resolution PV generation. This approach enables a consistent representation of coupled electrical and thermal energy flows in prosumer configurations and, differently from most previous works, explicitly captures the interaction between on-site PV

generation, reversible HP operation in both heating and cooling modes, and bidirectional energy exchange with DHCNs.

- Specific attention is devoted to Mediterranean climate conditions, where high cooling demand and strong solar availability significantly influence system performance. This aspect is often overlooked in the literature, which is predominantly focused on heating-dominated regions. Furthermore, the work provides a comparative assessment of alternative strategies for the valorisation of surplus PV electricity, namely direct grid export and conversion into thermal energy for supply to the district network, thereby offering a structured framework to analyse prosumer operation in sector-coupled energy systems.
- Finally, the economic feasibility of the proposed configuration is investigated under different electricity and thermal energy pricing schemes through dedicated sensitivity analyses, providing insights into the conditions required for the effective deployment of PV-driven thermal prosumers.

The remainder of the paper is structured as follows. Section 2 describes the case study and the modelling methodology. Section 3 presents the investigated scenarios and the main assumptions. Section 4 discusses the energy and economic results, while Section 5 summarizes the main conclusions.

MATERIALS AND METHOD

Description and modelling of the reference building

The case-study office building follows the reference specifications provided by ASHRAE Standard 90.1-2016 [44]. The methodology adopted for the modeling and simulation of the building has been previously described in a publication by some of the authors [45]; however, the main assumptions are briefly recalled here to ensure the self-consistency of the present work. First, the building is assumed to be situated in Palermo, in Southern Italy, and is composed of three floors above ground, with a floor-to-floor height of 3.96 m. Each level is divided into a central core zone and four perimeter zones. The glazed areas amount to 43 m² on the north and south façades, and 28.63 m² on the east and west façades. The thermal transmittance of opaque and transparent envelope elements is summarized in Table 1; values were adjusted to reflect Italian building practice in accordance with UNI/TR 11552:2014 [46]. Occupancy density, as well as lighting and equipment power densities, are also collected in Table 1. Operating schedules for occupants, lighting, and equipment are defined daily, distinguishing between weekdays and weekends, and are derived from the profiles specified in ASHRAE 90.1-2016 [44]. The building was simulated in TRNSYS [15], with Outdoor Air temperature (ODT) for Palermo retrieved from the Meteonorm Database. The resulting cooling and heating demands are shown in Figure 1.

Table 1. Details of the reference office building [45].

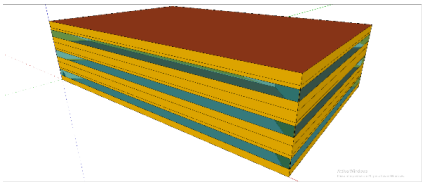

Geometrical properties and internal gains of the building according to ASHRAE 90.1	
Net conditioned floor area [m²]	1083
Number of floors	3
Window-Wall-Ratio (WWR) [%]	33
Number of thermal zones	18
Lighting [W/m²]	11
Electric equipment [W/m²]	8
Occupants [m²/person]	19
Thermal properties according to UNI/TR 11552: 2014	
Ground [W/m²K] - Code entity	1.26 - SOL08
External wall [W/m²K] - Code entity	1.43 - MPF01
External roof [W/m²K] - Code entity	1.62 - COP04
Adjacent wall [W/m²K] - Code entity	1.18 - MLP03

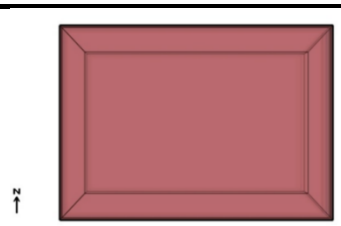

Adjacent ceiling [W/m^{2}K] - Code entity	1.92 - SOL02
Windows [W/m^{2}K] - Code entity	2.83 -WinID 1002 TRNSYS library

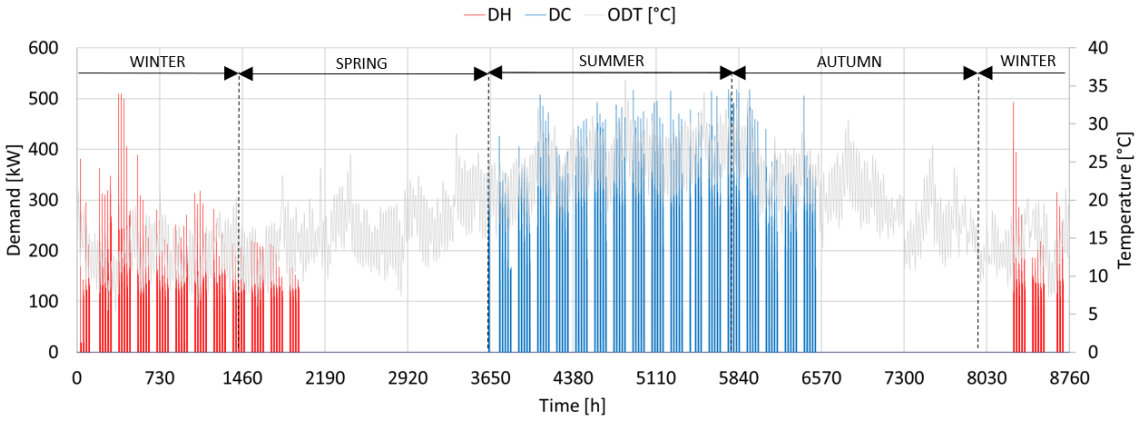

Figure 1. Heating and cooling demand for the office building [45].

Description and modelling of the air-conditioning plant

The description and modeling of the hydronic plant were already presented in previously published work by some of the authors [45]. For the sake of self-consistency, only the main features are briefly recalled here, while the reader is referred to the cited paper for a more detailed description and discussion.

The air-conditioning plant consists of two hydraulic loops, namely a primary and a secondary circuit, and includes a reversible air-to-water HP, a thermal energy storage tank, and a circulation pump. The secondary water loop is responsible for distributing heated and chilled water throughout the building and consists of circulation pumps, mixing and diverting valves, distribution piping, and fan coil units serving each thermal zone. The entire thermal system—ranging from the heat HP to the terminal fan coil units, as well as the building envelope and the thermal zones—was implemented in TRNSYS.

The nominal cooling and heating capacities of the air-to-water HP were respectively equal to 321 kW_c and 390 kW_{th}, based on the standard rating conditions [47]. Table 2 summarizes the technical data available from a commercial catalogue.

Table 2. Technical details on the reference air-to-water HP.

Refrigerant Circuit	**Details**
Refrigerant	R410a
Condenser Type	Fin and Tube
Number of Condensers	2
Condenser Fan Power [kW]	8
Metering Device	Electronic Expansion Valve
Evaporator Water Flowrate [m^3/h]	55.4
Evaporator Pump Power [kW]	6
Compressor Type (and Number)	Scroll (4)
Compressor Power (each) [kW]	37

The HP modeling was developed following an approach previously validated by the authors [48]. The simulations were carried out using IMST-Art software (version 4.0)[49], whose reliability in describing vapor-compression systems has been widely documented in the literature [50–53]. The HP performance in cooling modes was described through Equations (1) and (2), which were used to evaluate the delivered cooling capacity and the corresponding electrical power consumption [48].

$$CC = a_1 N_{CMP} + a_2 T_{wr} + a_3 ODT \quad (1)$$

$$P_{e,C} = b_1 N_{CMP} + b_2 T_{wr} + b_3 ODT \quad (2)$$

Table 3 collects all the fitting coefficients for Equations 1 and 2, together with Root Mean Square Error (RMSE) and Normalized Root Mean Square Error (NRMSE). Similar equations were developed for the heating capacity and absorbed power. For the sake of brevity, only fitting coefficients are shown in Table 3.

Table 3. Regression coefficients for the HP performance correlations (cooling/heating): delivered capacity and absorbed power models, including RMSE and NRMSE of the fitted datasets.

	Delivered Capacity			Absorbed Power		
Cooling	a_1	76.68	RMSE [kW]: 1.55 NRMSE [%]: 1.15	b_1	37.66	RMSE [kW]: 0.3 NRMSE [%]: 2.33
	a_2	6.70		b_2	-1.95	
	a_3	-1.86		b_3	0.63	
Heating	a_1	100.17	RMSE [kW]: 3.0 NRMSE [%]: 1.16	b_1	30.59	RMSE [kW]:0.3 NRMSE [%]:0.98
	a_2	-1.06		b_2	0.36	
	a_3	5.10		b_3	-0.51	

Electrical demand of the reference building

The electrical demand of the building is divided into two components: mandatory office loads and HP electricity consumption. Figure 2 shows the weekly electrical demand profile associated with mandatory office loads, i.e., all electrical uses excluding space conditioning provided by the HP [44]. The demand exhibits a clear weekday-weekend pattern, with pronounced peaks during working hours from Monday to Friday, corresponding to typical office activities such as lighting, IT equipment, and auxiliary systems. During weekdays, peak demand reaches approximately 120 kW, while nighttime consumption remains limited to base-load levels. On Saturday, both the peak magnitude and duration are reduced, reflecting partial occupancy and limited operational schedules. In contrast, Sunday demand is almost constant and significantly lower, indicating minimal building usage.

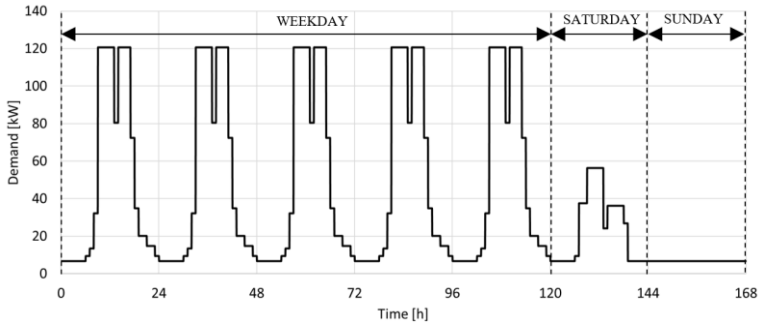

Figure 2. Weekly electrical demand profile associated with mandatory office loads [44].

Figures 3-a.b illustrate the electrical demand of the air-to-water HP (red solid curve) for two typical days of the year: one in winter (January 16th) and one in summer (August 4th). The stepwise pattern of the HP electricity demand reflects the sequential activation of the four compressors, with on-off cycling shown in Figures 3.c-d. Looking at Figure 3.c, during the heating season, compressors' operation is driven by the temperature of the upper node of the thermal energy storage. A temperature setpoint of 50 °C with a ±2.5 °C deadband is adopted: as the storage temperature decreases, compressors are progressively activated, while they are sequentially switched off when the temperature rises above the upper threshold. Figures 3.b and 3.d show the corresponding results for a summer operating condition. In this case, the monitored variable is the temperature at the lower node of the storage, representative of the cooling operation, with a setpoint of 7 °C and a ±1 °C deadband. Similar to the winter case, the compressor activation sequence follows the deviation of the storage temperature from the setpoint, resulting in a modulated electrical demand of the HP. Overall, the figures highlight the strong coupling between storage temperature control, compressor sequencing, and electrical demand profiles, as well as the distinct operational behavior of the system under heating and cooling conditions.

The simulations showed that the total annual electricity consumption of the building is equal to 408,194.10 kWh·yr^{-1}. Of this amount, 353,439.99 kWh·yr^{-1} (86.59%) are related to mandatory electricity uses, such as lighting and equipment in the thermal zones, while the remaining 54,754.11 kWh·yr^{-1} (13.41%) are required for the operation of the HP.

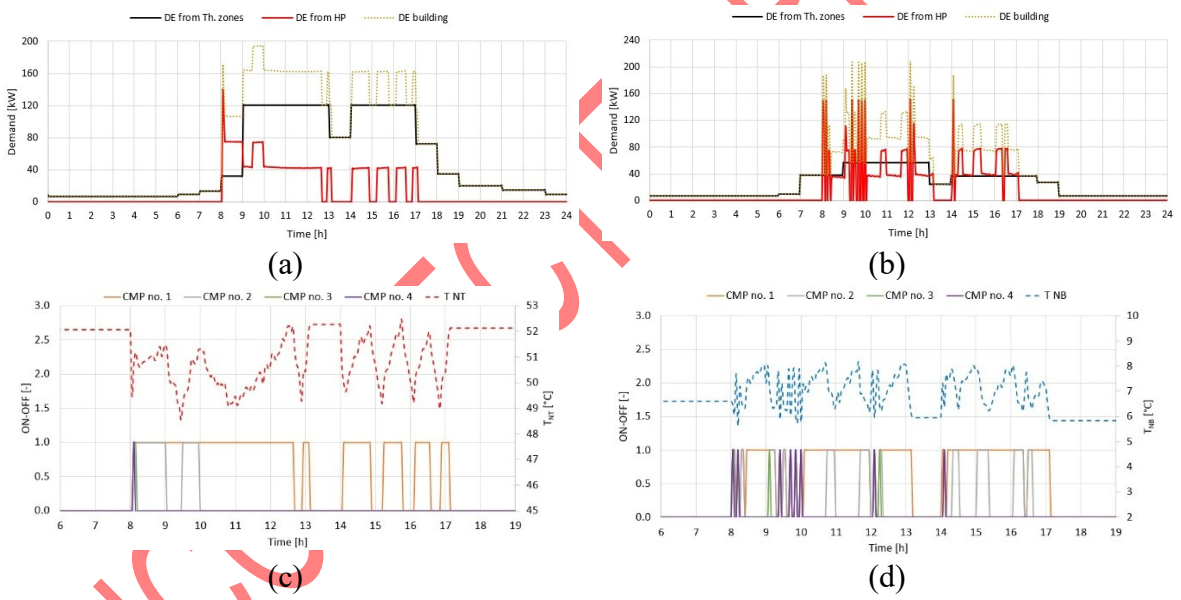

Figure 3. HP electricity demand and control behaviour for two representative days: winter operation (January 16th) and summer operation (August 4th). (a) Winter: HP electrical demand and mandatory office loads. (b) Summer: HP electrical demand and mandatory office loads. (c) Winter: compressor staging (four compressors) and thermal storage upper-node temperature with a 50 °C setpoint and ±2.5 °C deadband. (d) Summer: compressor staging and thermal storage lower-node temperature with a 7 °C setpoint and ±1 °C deadband.

Photovoltaic system modelling and methodology for layout optimization

To assess the feasibility and optimal sizing of a rooftop PV system for the non-residential building under study, a dedicated Python-based simulation and optimization workflow was developed. The proposed methodology integrates geometric constraints of the available roof area, component specifications, meteorological inputs, and electrical load profiles to identify the PV configuration that maximizes on-site energy utilization and minimizes grid dependence. To better understand the procedure, the overall simulation and optimization workflow is schematically

summarized in the block diagram reported in Figure 4, illustrating the interaction between geometric layout generation, PV performance modelling, load matching, and optimization loop.

The flat rooftop was parameterized according to its effective geometric dimensions (49.92 m east-west, 33.29 m north-south), accounting for mandatory setbacks, maintenance corridors, and row spacing constraints. The PV layout was discretized by defining two decision variables: the number of module rows N_r (north-south direction), and the number of modules per row N_m (east-west direction). For each feasible pair (N_r, N_m), the total number of installed modules and the corresponding DC peak power were computed based on the selected commercial PV module (550 W_p, 2.10 m × 1.13 m).

Row spacing (pitch) was determined to prevent inter-row shading at solar noon during the winter solstice, adopting a conservative geometric criterion. For each feasible layout (N_r, N_m), the total number of installed modules, the corresponding DC peak power, and the ground coverage ratio were calculated. Configurations violating geometric or electrical constraints were discarded a priori. For each admissible configuration, inverter sizing was automatically performed to match the DC capacity while respecting practical DC/AC ratio limits, selecting commercially available inverter units, and aggregating their nominal AC power.

PV energy production was simulated using the open-source *pvlib* Python library. Consistent with the building simulation, meteorological inputs were derived from the PVGIS Typical Meteorological Year (TMY) dataset for Palermo [16], providing hourly values of global horizontal irradiance (GHI), direct normal irradiance (DNI), diffuse horizontal irradiance (DHI), ambient temperature, and wind speed. Plane-of-array irradiance was computed for each configuration, and module cell temperature was estimated using the Sandia Array Performance Model (SAPM), considering an open-rack glass-glass module. DC power production was calculated through the PVWatts performance model, accounting for irradiance and temperature effects, while AC power output was obtained by applying inverter efficiency and clipping effects [54]. The resulting PV AC power time series was generated at hourly resolution and aligned with the building electrical load profile.

For each candidate configuration, the hourly energy balance was evaluated as:

$$P_{bal}(t) = P_{load}(t) - P_{PV}(t) \tag{3}$$

where $P_{load}(t)$ represents the electrical load of the building and $P_{PV}(t)$ is the PV system's AC power output at time t. The annual electricity imported (E_{import}) from the grid was computed as:

$$E_{import} = \sum_{t=1}^{T} \max[P_{load}(t) - P_{PV}(t), 0]\,\Delta t \tag{4}$$

where T denotes the total number of hours in the year and $\Delta t = 1\ h$. While the annual electricity surplus that is exported to the grid (E_{export}) was computed as:

$$E_{export} = \sum_{t=1}^{T} max[P_{PV}(t) - P_{load}(t), 0]\,\Delta t \tag{5}$$

Based on the hourly energy balance, a set of energy-related key performance indicators (KPIs) was computed. The annual PV energy production (E_{PV}) and the annual building electrical demand (E_{load}) were obtained by integrating the corresponding hourly profile. The amount of self-consumed PV electricity (E_{self}) was defined as:

$$E_{self} = \sum_{t=1}^{T} min[P_{PV}(t), P_{load}(t)]\,\Delta t \tag{6}$$

From these quantities, the self-consumption ratio (SCR) and the load coverage factor (LCF) were calculated as follows:

$$SCR = \frac{E_{self}}{E_{PV}} \quad (7)$$

$$LCF = \frac{E_{self}}{E_{load}} \quad (8)$$

The PV system sizing problem was formulated as a discrete optimization over the set of geometrically feasible layouts, to minimize the annual electricity imported from the grid (i.e., $min\, E_{import}$)

This criterion was selected to directly enhance on-site utilization of PV generation and reduce dependence on external electricity supply, which is particularly relevant for non-residential buildings characterized by significant daytime electrical loads. The remaining KPIs were used to characterize the performance of the optimal configuration, but did not directly enter the objective function.

The energy KPIs associated with the optimal PV configuration were subsequently used as input for the economic assessment of the integrated PV-HP-DHCNs. Annual revenues were computed by distinguishing between self-consumed electricity, valued as avoided electricity purchase, surplus electricity exported to the grid, and surplus electricity converted into thermal energy through the air-to-water HP and sold to the district heating and cooling network. The annual cash flow in the *y-th* year was defined as follows:

$$CF_y = R_y - OPEX_y - REINV_y \quad (9)$$

where R_y represents total annual revenues, $OPEX_y$ the operating expenditures, and $REINV_y$ possible reinvestment costs.

The Net Present Value (NPV) over the system lifetime (N) was calculated as:

$$NPV = \sum_{y=0}^{N} \frac{CF_y}{(1+r)^y} \quad (10)$$

where r is the discount rate. The Internal Rate of Return (IRR) was obtained as the value of r satisfying:

$$0 = \sum_{y=0}^{N} \frac{CF_y}{(1+IRR)^y} \quad (11)$$

Finally, discounted payback time was evaluated based on the cumulative nominal and discounted cash flows.

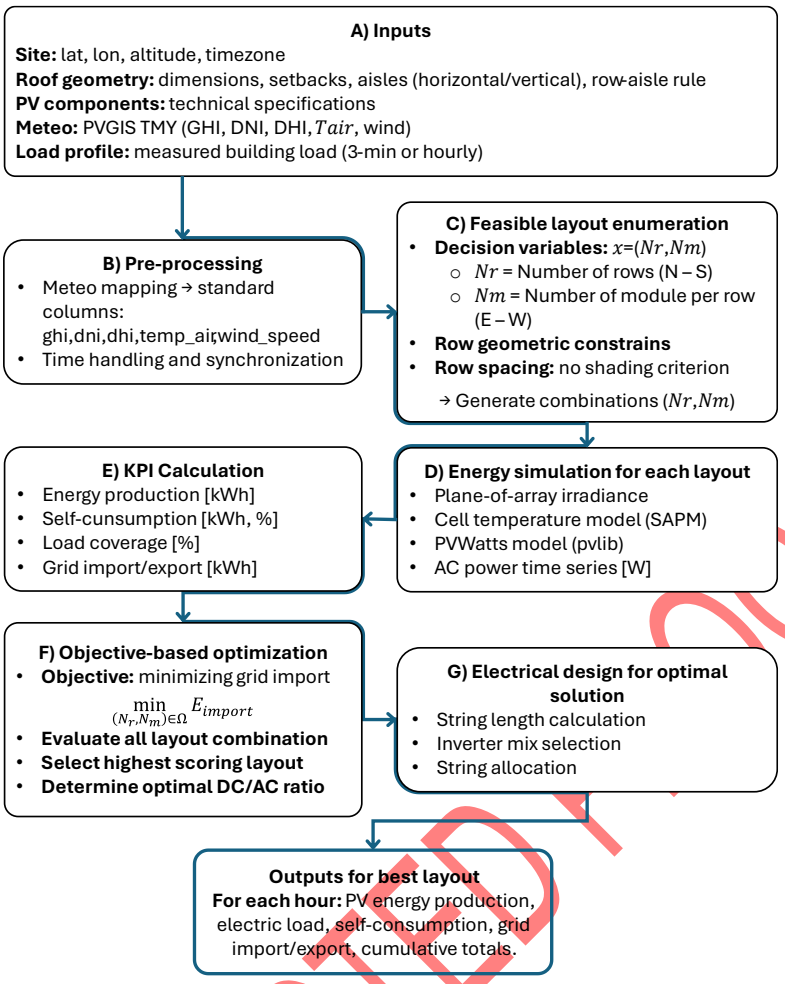

Figure 4. Description of the optimization routine for sizing of the PV plant.

Investigated scenarios and main assumptions

Figure 5 provides a schematic layout of the PV system installed on the roof of the office building, highlighting the usable area and access aisles. The PV plant supplies electricity to a dedicated air-to-water HP, which converts surplus PV power into heat or cold for on-site use and for export to the DHCN through a heat exchanger.

Two scenarios are analysed:

- *Electricity Surplus to the grid*: all surplus PV electricity is sold to the electrical grid at a given selling price.
- *Thermal prosumer:* surplus PV electricity is supplied to a "dedicated and newly installed" air-to-water HP, which produces hot water at 40-45 °C during the heating season (December–March) and chilled water at 6 °C during the cooling season (May–September), with the generated thermal energy exported to the DHCN. As shown in Eqs 12-13, the Coefficient of performance (COP) and the Energy Efficiency Ratio (EER) of the HP were parameterized using quadratic correlations derived from the performance of representative medium-size commercial units with nominal capacity between 250-300 kW, modelled by IMST-Art, accounting not only for the effect of ODT but also for the progressive reduction of thermal demand from the DHCN at milder ODTs, which influences the effective operating conditions and part-load efficiency of the machine.

$$EER(ODT) = 0.027\ ODT^2 - 1.742\ ODT + 30.434 \quad (12)$$

$$COP(ODT) = 0.018\,ODT^2 - 0.036\,ODT + 4.952 \quad (13)$$

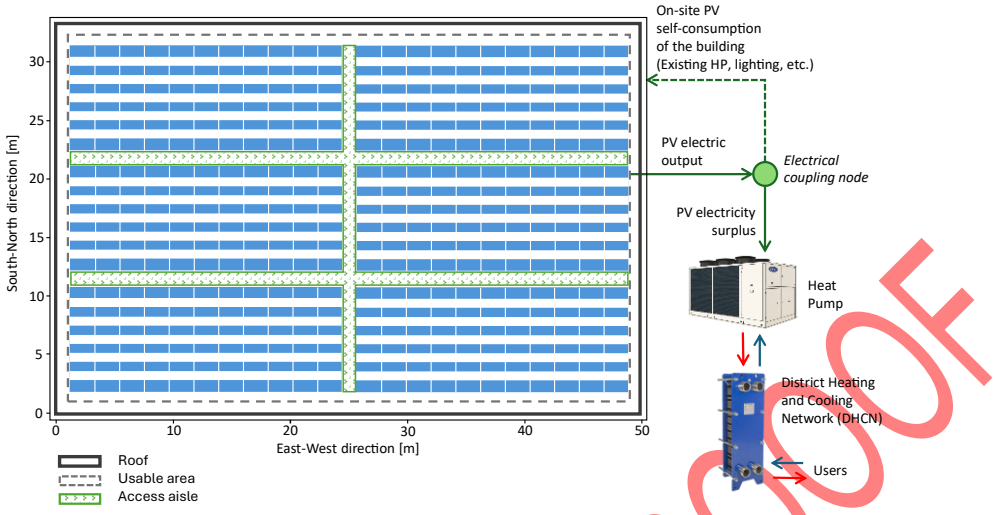

Figure 5. Detailed energy flow exchanges between the PV plant and the HP used to provide heat & cold to a local DHCN.

The economic analysis of the proposed PV system was carried out over a lifetime horizon of 25 years, assuming a weighted average cost of capital (WACC) of 7% as the discount rate. The initial investment cost (CAPEX) was estimated at 1400 €/kW$_p$, inclusive of modules, inverters, installation, and balance-of-system, while annual operating expenditures (OPEX) were considered equal to 4% of CAPEX. A reinvestment equal to 10% of CAPEX was included in year 12 to account for inverter replacement or other revamping operations. Energy production was corrected by an annual performance degradation of 0.5%. The economic valorization of electricity was distinguished between self-consumed energy, valued at 0.15 €/kWh (avoided cost of electricity purchase), and surplus electricity exported to the grid, valued at 0.11 €/kWh. The latter reflects the average remuneration, which represents typical market schemes in the Italian regulatory context. For the case of the air-to-water HP, a CAPEX of about 250 €/kW$_c$ was assumed [55]. Furthermore, it was assumed a selling price of heat/cold of about 0.05 €/kWh.

All tariffs were assumed to grow annually at a nominal rate, compounding an inflation rate of 2% and a real escalation factor of 1.5%, resulting in an effective annual growth of approximately 3.5%. OPEX was assumed to escalate at the inflation rate only (2% per year). No fiscal incentives or tax effects were applied to maintain the analysis conservative and technology-focused. On this basis, yearly revenues, OPEX, and cash flows were computed, and the main financial indicators were derived, including Net Present Value (NPV), Internal Rate of Return (IRR), and Discounted Payback Time (DPBT).

Two sensitivity analyses were carried out to evaluate the robustness of the results with respect to key tariff parameters. The first analysis focused on the effect of the heat and cold selling price, varying it from the reference value of 0.05 €/kWh to 0.08 €/kWh and 0.11 €/kWh, to reflect different market and regulatory conditions. The second analysis investigated the impact of electricity price variability on both scenarios, by varying the self-consumption tariff—assumed equal to the avoided cost of grid electricity purchase—between 0.09 €/kWh (−40% relative to the baseline of 0.15 €/kWh) and 0.21 €/kWh (+40%), thus accounting for the significant volatility observed in electricity markets in recent years.

RESULTS AND DISCUSSION

First, the optimal solution identified by the optimization procedure consists of 18 module rows and 22 modules per row, corresponding to a total of 396 PV modules and a DC installed capacity

of approximately 217.8 kW_p. The selected inverter configuration includes four 50 kW units, resulting in a total AC capacity of 200 kW and a DC/AC ratio of 1.09. It is important to note that, given the adopted optimization criterion, namely the minimization of annual electricity imports from the grid, and the absence of penalties associated with surplus generation, the optimal solution naturally converges towards the maximum PV capacity installable on the available rooftop area, subject to geometric and technological constraints.

Results for typical days

Figure 6 illustrates the electrical energy flows among the PV system, the HP, and the DHCN for two representative operating days: a winter day (January 16th, Figure 6a) and a summer day (August 4th, Figure 6b). During the winter day, PV electricity production is limited and mainly concentrated around midday, covering only a small fraction of the HP electrical demand (below 20%), which is therefore largely supplied by electricity imported from the grid during heating operation. Conversely, during the summer day, higher solar irradiance leads to a significant increase in PV generation, allowing more than 60-70% of the HP electrical demand to be directly supplied by on-site PV production during peak hours. As a result, a substantial PV surplus is observed, especially around midday, which can be exported to the grid or indirectly exploited through cooling production and interaction with the DHCN. Overall, the comparison highlights the strong seasonal variability of PV-driven prosumer operation and the role of HP and DHCN in enhancing PV self-consumption and system flexibility.

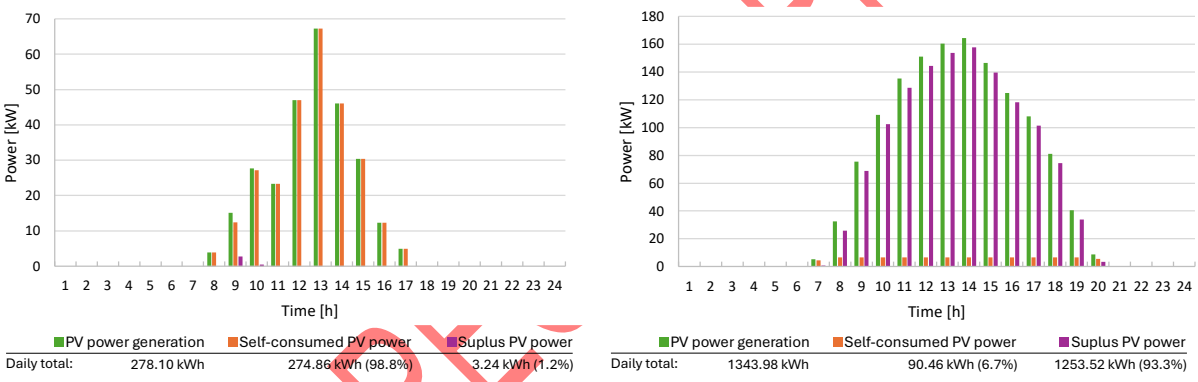

(a) (b)

Figure 6. Hourly electrical power flows among the PV system, HP, and grid/DHCN interface for two representative days: winter day (January 16th) (a) and summer day (August 4th) (b).

Energy results for one year of operation are presented in Figures 7a and 7b. Figure 7a shows the hourly electricity surplus, highlighting a clear seasonal trend, with higher values during summer and peak values of approximately 185 kW. On an annual basis, the system achieved a PV generation of 363,109 kWh, covering 53.9% (LCF) of the building's annual electricity demand (408,193 kWh). Of the PV generation, 220,239 kWh were self-consumed on-site (self-consumption ratio SCR = 60.7%), while 142,869 kWh were exported to the grid. Consequently, annual grid imports were reduced to 187,954 kWh.

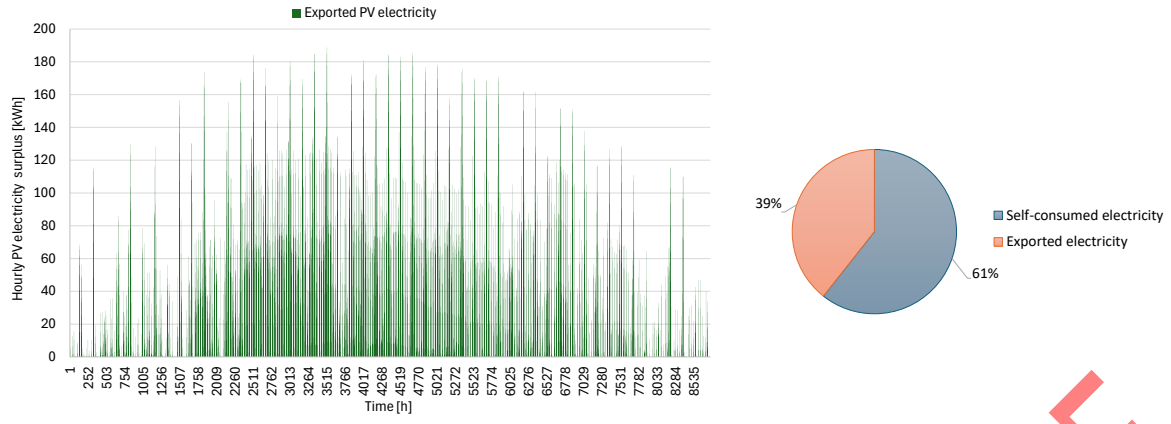

(a) (b)

Figure 7. PV surplus and annual energy balance for the optimal PV layout. Hourly profile of PV surplus power over the year (a). Annual PV energy balance showing self-consumed electricity, exported electricity, and resulting grid imports (b).

Figure 8.a shows the power flows in the thermal prosumer scenario, including HP heating and cooling output exported to the DHCN, and surplus PV power, which is exported to the grid when the HP connected to the DHCN is switched off. During the winter and mid-season periods, the system mainly operates in heating mode, with HP thermal power peaks reaching 450 kW. In these periods, PV surplus power is limited and occurs primarily during daytime hours in spring and autumn, with exported power typically below 150 kW. Conversely, during the summer, cooling operation dominates, with the HP reaching peak values of approximately 476 kW during high cooling demand conditions. In this period, the higher availability of solar generation leads to increased PV surplus, which can be either exported to the grid when the HP is inactive or indirectly valorized through cooling production and interaction with DHCN.

Figure 8.b shows monthly and yearly results. The system generates 47.03 MWh y^{-1} of heat and 168.52 MWh y^{-1} of cooling. This is mainly driven by the higher availability of PV electricity during the summer season compared to winter, resulting in a greater production of chilled water supplied to the DHCN, which is particularly beneficial in cooling-dominated climates. Meanwhile, the surplus electricity exported to the grid amounts to 72.19 MWh·y^{-1}

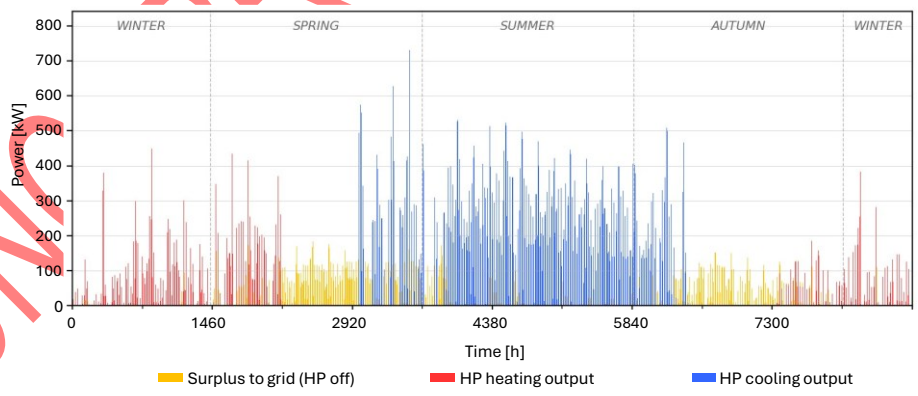

(a)

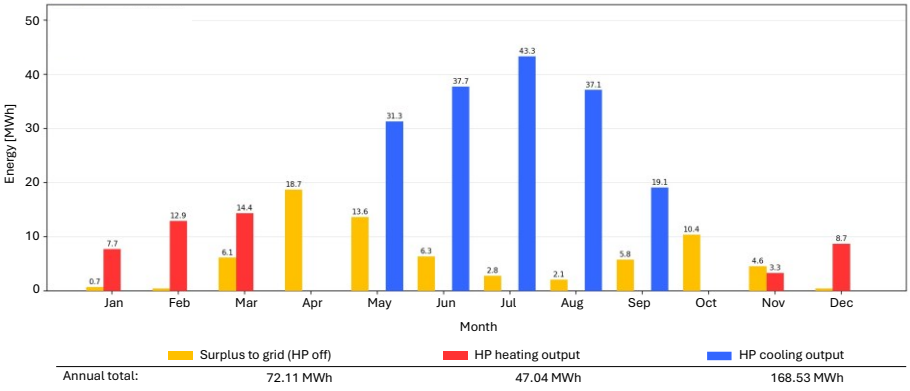

(b)

Figure 8. Thermal prosumer operation: (a) hourly profiles of PV surplus electricity, and corresponding heat and cooling outputs delivered by the dedicated HP to the district heating and cooling network; residual electricity export to the grid when the dedicated HP is off; and (b) monthly and yearly energy results.

Economic results and sensitivity analysis

Figure 9 compares the economic performance of the "Electricity surplus to the grid" and "Thermal prosumer" scenarios in terms of Net Present Value, Discounted Payback Time, and Internal Rate of Return.

Results show that the electricity surplus to the grid scenario achieves the highest economic performance, with an NPV of approximately 350 k€, a DPBT of about 9 years, and an IRR of 16.21%. This outcome is mainly driven by lower system complexity (absence of the additional HP and connection to the DHCN) and the direct monetization of PV surplus electricity through grid export. In contrast, the thermal prosumer scenario yields a lower but still attractive profitability, with an NPV of around 240 k€, a DPBT of approximately 13-14 years, and an IRR of 11.90%. The reduction in economic indicators is associated with higher initial investment and operational complexity related to the HP operation and thermal interaction with the DHCN. However, this scenario enables the provision of flexible thermal services to the district network and power grid, which are not fully captured by purely economic metrics. Overall, the comparison highlights a trade-off between short-term economic profitability and system-level benefits, suggesting that the thermal prosumer configuration may become increasingly attractive under future market conditions with higher electricity prices, increased remuneration of flexibility services, or stronger incentives for sector coupling.

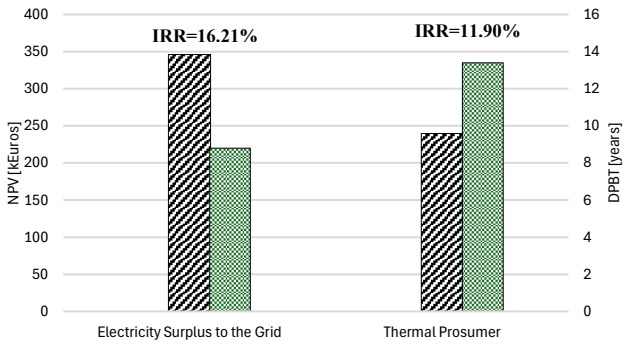

Figure 9. Economic performance comparison between the electricity export and thermal prosumer configurations in terms of NPV, DPBT, and IRR.

The sensitivity of the main economic KPIs (NPV, IRR, and DPBT) to two key tariff parameters is reported in Tables 4 and 5, which examine the effect of the heat and cold selling price and the self-consumption electricity tariff, both for the electricity surplus to the grid and the thermal prosumers scenarios.

Regarding the heat and cold selling price, results confirm that this parameter exclusively affects the thermal prosumer configuration, as no dedicated HP is operated in the electricity surplus to the grid scenario, whose KPIs therefore remain fixed at the reference values (NPV = 346 k€, IRR = 16.2%, DPBT = 8.8 years) regardless of the assumed thermal tariff. The selling price of heat/cold was varied from 5c€/kWh (reference case) up to 11c€/kWh. As shown in Table 4, for the thermal prosumer, increasing the selling price from 5 c€ kWh^{-1} (reference case) to 11 c€ kWh^{-1} raises the NPV from 239.78 k€ to 438.63 k€ and the IRR from 11.9% to 15.5%. At the same time, the DPBT decreases from 13.4 years to 9.4 years, confirming the strong sensitivity of this scenario to thermal energy remuneration.

Table 4. Sensitivity analysis of key economic indicators (NPV, IRR, and DPBT) to the assumed heat/cooling selling price in the thermal prosumer scenario.

Heat & Cold Selling price	**NPV**	**IRR**	**DBPT**
[€/kWh]	[k€]	[%]	[Years]
0.05 (Reference case)	239.78	11.9%	13.40
0.08	339.20	13.7%	10.83
0.11	438.63	15.5%	9.36

On the other hand, regarding the self-consumption electricity tariff, both scenarios are significantly affected, as self-consumed PV electricity represents the dominant revenue component in both configurations, amounting to 220,239 kWh yr^{-1}. As shown in Table 5, varying the tariff between 9 c€ kWh^{-1} (−40% relative to the baseline of 15 c€ kWh^{-1}) and 21 c€ kWh^{-1} (+40%) produces a wide range of outcomes. For the electricity surplus to the grid scenario, the NPV spans from 142.8 k€ to 549.1 k€, with the IRR ranging between 11.1% and 20.9% and the DPBT between 6.5 and 14.6 years. The thermal prosumer scenario exhibits a similar directional response, with NPV ranging from 36.6 k€ to 442.9 k€, IRR from 7.8% to 15.5%, and DPBT from 9.3 to 22.1 years. Notably, at the lowest tariff level (9 c€ kWh^{-1}), the thermal prosumer IRR of 7.8% falls marginally above the assumed WACC of 7%, indicating that economic viability is maintained but with limited margin. This result underscores that the thermal prosumer configuration is more exposed to unfavourable electricity market conditions, given the combined effect of higher investment cost and lower revenue diversification at reduced tariff levels. Overall, the self-consumption electricity tariff emerges as the most influential economic driver for both scenarios, reinforcing the importance of stable and favourable regulatory frameworks for distributed PV generation in the Mediterranean context.

Table 5. Sensitivity of key economic indicators (NPV, IRR, and DPBT) to self-consumption electricity tariff.

	Electricity surplus to the grid			**Thermal prosumer**		
Electricity purchase price	**NPV**	**IRR**	**DBPT**	**NPV**	**IRR**	**DBPT**
[€/kWh]	[k€]	[%]	[years]	[k€]	[%]	[years]
0.09	142.79	11.11	14.63	36.62	7.81	22.05
0.15 (Reference case)	345.95	16.21	8.79	239.78	11.89	13.41
0.21	549.11	20.92	6.45	442.94	15.54	9.31

Limitations of the present study and future remarks

Despite the comprehensive energy and economic assessment presented in this work, some limitations should be acknowledged.

- First, the analysis is based on a single non-residential case study located in a Mediterranean context. While representative of Southern European conditions, results may differ for other building typologies, occupancy profiles, or DHCN configurations. Future studies should extend the analysis to residential and mixed-use buildings and to districts with multiple interacting prosumers.
- Second, the economic evaluation relies on assumed electricity, heat, and cold prices, reflecting current market conditions. Although a sensitivity analysis was conducted on heat and cold selling prices, future electricity market dynamics, policy incentives, and regulatory mechanisms were not explicitly modelled. Further research should investigate dynamic pricing schemes, flexibility markets, and alternative business models for PV-HP-based prosumers in DHCNs.
- Third, the substation and DHCN interaction were modelled in a simplified manner, focusing on aggregated energy flows. Detailed thermo-hydraulic behavior, heat exchanger performance, pressure drops, and advanced control logics were not explicitly represented. Future work should integrate detailed substation and network models to assess hydraulic constraints, temperature management, and coordinated operation among multiple prosumers. Moreover, capital expenditures related to the substation should be included to enable a comprehensive techno-economic evaluation.
- Finally, the HP operation was governed by rule-based control strategies. Advanced control approaches, such as model predictive control or AI-based energy management, could further enhance PV self-consumption, reduce peak loads, and improve both economic and system-level performance.

CONCLUSIONS

This work presented a comprehensive energy and economic assessment of a PV-driven air-to-water HP operating as a thermal prosumer in a Mediterranean office building connected to a DHCN. By combining detailed building energy modelling, dynamic HP performance characterization, and optimized PV system sizing, the study provides an integrated evaluation framework tailored to Southern European climatic conditions, where cooling demand and solar availability play a dominant role. Results demonstrate a strong seasonal complementarity between PV generation and cooling demand, enabling an effective valorization of surplus PV electricity through thermal energy production. On an annual basis, the system supplies 47.03 MWh of heat and 168.52 MWh of cooling to the DHCN, while still exporting 72.19 MWh of electricity to the grid. This highlights the dual role of the prosumer configuration in both supporting the electricity system and providing renewable thermal services to the district network. From an economic perspective, the direct export of surplus electricity currently yields higher profitability due to lower investment complexity, with an IRR of 16.2% and a discounted payback time of 8.8 years. However, the thermal prosumer configuration proves economically viable under suitable heat and cold remuneration schemes, with IRR values increasing from 11.9% to 15.5% as the selling price rises from 5 to 11 c€ kWh^{-1}, and discounted payback times decreasing from 13.4 to 9.4 years accordingly. A second sensitivity analysis was carried out on the self-consumption electricity tariff, defined as the avoided cost of grid electricity purchase. The results indicate that this parameter represents the most influential economic driver for both configurations. Varying the tariff between 9 c€ kWh^{-1} (−40%) and 21 c€ kWh^{-1} (+40%) relative to the baseline of 15 c€ kWh^{-1} produces a wide range of outcomes: for the electricity surplus to the grid scenario, the IRR spans from 11.1% to 20.9%, while for the thermal prosumer the IRR ranges from 7.8% to 15.5%. Notably, at the lowest tariff level, the thermal prosumer IRR falls only marginally above the assumed WACC of 7%, underscoring the heightened exposure of this configuration to unfavorable electricity market conditions. This is a relevant finding given the high volatility of energy prices observed in the Mediterranean region in recent years. Overall, these results underline the critical role of both thermal energy pricing mechanisms and electricity market stability in

enabling the economic viability and diffusion of renewable-based thermal prosumers. Overall, the findings confirm that PV-driven HPs represent a technically mature and flexible solution for integrating renewable electricity into DHCNs in Mediterranean contexts. By enhancing PV self-consumption, reducing grid imports, and supplying low-carbon heat and cold, thermal prosumers can contribute to sector coupling and system flexibility. From a policy and system perspective, the results of this study highlight several relevant implications. For policymakers, the findings emphasize the importance of appropriate remuneration schemes for thermal energy, as the economic viability of PV-driven thermal prosumers strongly depends on the valuation of heat and cold supplied to DHCN. Support mechanisms targeting sector coupling and renewable-based thermal services may therefore play a key role in accelerating their deployment. For network operators, the integration of PV-driven HPs at the building level represents an opportunity to enhance system flexibility and reduce renewable energy curtailment, although it requires careful management of bidirectional energy flows and seasonal imbalances between electricity production and thermal demand. Finally, for system planners, the results underline the need to consider the joint design of building-integrated PV systems, HPs, and DHCNs, accounting for local climatic conditions, demand profiles, and market structures, to fully exploit the potential of thermal prosumers within future low-carbon energy systems. Future research should focus on multi-prosumer interactions at the district scale, advanced control strategies, and the integration of flexibility and ancillary service markets, which are expected to further improve both the economic and system-level value of such configurations.

ACKNOWLEDGMENTS

This study was developed in the framework of the research activities carried out within:

- the PRIN 2020 project: "OPTIMISM—Optimal refurbishment design and management of small energy micro-grids", CUP: B73C22000320001, funded by the Italian Ministry of University and Research (MUR).
- the Project "Network 4 Energy Sustainable Transition - NEST", Spoke 7: Smart Sector Integration, Project code PE0000021, CUP: B73C22001280006, funded under the National Recovery and Resilience Plan (NRRP), Mission 4, Component 2, Investment 1.3 - Call for tender No. 1561 of 11.10.2022 of Ministero dell'Università e della Ricerca (MUR); funded by the European Union - NextGenerationEU.

NOMENCLATURE

Symbols

$\dot{m}_w$	Water mass flow rate	[kg s^{-1}]
CF_y	Cash flow in the year y	[€]
E_{PV}	annual photovoltaic energy production	[kWh]
E_{export}	annual electricity exported to the grid	[kWh]
E_{import}	annual electricity imported from the grid	[kWh]
E_{load}	annual electrical demand	[kWh]
E_{self}	self-consumed PV electricity	[kWh]
$P_{PV}(t)$	PV AC power output at time	[kW]
$P_{load}(t)$	Electrical load at time t	[kW]
CC	Cooling Capacity	[W]
c_w	Specific heat capacity of water	[kJ/(kg °C)]
HC	Heating Capacity	[W]
N	System lifetime	[y]
N_m	number of modules per row	[-]
N_r	number of module rows	[-]
NRMSE	Normalized Root Mean Square Error	[%]

$OPEX_y$	Operating expenditures	[€/y]
r	discount rate	[-]
$REINV_y$	reinvestment costs	[€/y]
RMSE	Root Mean Square Error	[W]
R_y	total annual revenues	[€/y]
T	Total number of hours in the year	[h]
T_{wr}	Temperature of the water returning from the hydronic loop	[°C]
T_{ws}	Temperature of the water supplied to the hydronic loop	[°C]
$T_{ws,sp}$	Reference Temperature of the water supplied to the hydronic loop	[°C]

Greek letters

ω	Compressor rotational speed	[rpm]

Subscripts and superscripts

AC	Alternating current side
DC	Direct current side
export	Exported energy
hp	Heat pump
Import	Imported energy
load	Electric load
PV	Photovoltaic system
self	Self-consumption
y	Year

Abbreviations

CAPEX	Capital Expenditures
COP	Coefficient of Performance
DHCN	District Heating and Cooling Network
DHI	Diffuse Horizontal Irradiance
DNI	Direct Normal Irradiance
DPBT	Discounted Payback Time
EER	Energy Efficiency Ratio
GHI	Global Horizontal Irradiance
HP	Heat Pump
IRR	Internal Rate of Return
KPI	Key Performance Indicators
LCF	Load Coverage Factor
NPV	Net Present Value
NRMSE	Normalized Root Mean Square Error
ODT	Outdoor Air Temperature
P2C	Power-to-Cold
P2H	Power-to-Heat
PV	Photovoltaic
PVGIS	Photovoltaic Geographical Information System
RES	Renewable Energy Source
RMSE	Root Mean Square Error
SAPM	Sandia Array Performance Model
SCR	Self-Consumption Ratio

TMY Typical Meteorological Year
TRNSYS TRaNsient SYstem Simulation software
WACC Weighted Average Cost of Capital

REFERENCES

[1] Joint Research Centre (JRC) EC. Smart Thermal Networks in the European Union. Luxembourg: Publications Office of the European Union; 2023.
[2] Yuan M, al. et. Renewable energy and waste heat recovery in district heating: Status, potential and policy schemes. Energy 2024.
[3] Jerez Monsalves J, Bergaentzlé C, Keles D. Waste-heat recovery utilisation for district heating systems under diverse pricing schemes: A bi-level modelling approach. Appl Energy 2024;375:124032. https://doi.org/10.1016/J.APENERGY.2024.124032.
[4] Yuan X, al. et. Data center waste heat for district heating networks: A review. Renewable and Sustainable Energy Reviews 2025.
[5] Pastore LM, Lo Basso G, Ricciardi G, de Santoli L. Synergies between Power-to-Heat and Power-to-Gas in renewable energy communities. Renew Energy 2022;198:1383–97. https://doi.org/10.1016/j.renene.2022.08.141.
[6] ENTSO-E. Study on Power and Heat Sectors: Interactions and Synergies. Brussels: 2023.
[7] Abdelghani D, Koohi-Fayegh S, Lund H, Sorknæs P. A review on optimization of district energy systems. Renewable and Sustainable Energy Reviews 2026;225:116041. https://doi.org/10.1016/J.RSER.2025.116041.
[8] Soleimani A, Davidsson P, Malekian R, Spalazzese R. Modeling hybrid energy systems integrating heat pumps and district heating: A systematic review. Energy Build 2025;329:115253. https://doi.org/10.1016/j.enbuild.2024.115253.
[9] Guo Y, Wang J, Wang S, Song W, Ma Z, Jiang S. Design and flexible operation study of a bidirectional thermal substation based on building thermal battery model in fifth generation heating and cooling systems. Appl Therm Eng 2025;281:128817. https://doi.org/10.1016/J.APPLTHERMALENG.2025.128817.
[10] Pipiciello M, Caldera M, Cozzini M, Ancona MA, Melino F, Di Pietra B. Experimental characterization of a prototype of bidirectional substation for district heating with thermal prosumers. Energy 2021;223:120036. https://doi.org/10.1016/j.energy.2021.120036.
[11] Angelidis O, Zinsmeister D, Ioannou A, Friedrich D, Thomson A, Ganslmeier U, et al. Development and experimental validation of a hydraulic design and control philosophies for 5th generation district heating and cooling networks. Energy 2024;308:132835. https://doi.org/10.1016/J.ENERGY.2024.132835.
[12] Testasecca T, Catrini P, Beccali M, Piacentino A. Dynamic simulation of a 4th generation district heating network with the presence of prosumers. Energy Conversion and Management: X 2023;20:100480. https://doi.org/10.1016/J.ECMX.2023.100480.
[13] Hassan MA, Araji MT. Building bridges: Unlocking cost savings through peer-to-peer trading between heat prosumers. Energy Build 2025;347:116327. https://doi.org/10.1016/J.ENBUILD.2025.116327.
[14] Bonelli G, Capone M, Verda V, Guelpa E. Modeling and Performance Evaluation of a District Heating Network with Integration of a Thermal Prosumer: A Case Study in Italy. Energies (Basel) 2025;18. https://doi.org/10.3390/en18225977.
[15] Ricci M, Gianaroli F, Artioli M, Beozzo S, Sdringola P. Multi-Step Artificial Neural Networks for Predicting Thermal Prosumer Energy Feed-In into District Heating Networks. Energies (Basel) 2025;18. https://doi.org/10.3390/en18246608.
[16] Sdringola P, Pipiciello M, Ricci M, Gianaroli F, Menegon D, Trentin F, et al. Prosumers and district heating: Experimental validation of strategies to improve thermal energy

production and consumption. Energy Build 2025;338:115713. https://doi.org/10.1016/J.ENBUILD.2025.115713.

[17] Zinsmeister D, Lickleder T, Christange F, Tzscheutschler P, Perić VS. A comparison of prosumer system configurations in district heating networks. Energy Reports 2021;7:430–9. https://doi.org/10.1016/J.EGYR.2021.08.085.

[18] Dino GE, Catrini P, La Villetta M, Piacentino A. A techno-economic analysis of a high vacuum solar system integrated into a prosumer-based district heating network. Energy 2025;330:136843. https://doi.org/10.1016/J.ENERGY.2025.136843.

[19] Gianaroli F, Ricci M, Sdringola P, Pipiciello M, Menegon D, Melino F. Innovative approach and numerical modeling to retrofit existing substations for bidirectional operation: Enabling thermal prosumer participation in District Heating Network. Appl Energy 2025;401:126698. https://doi.org/10.1016/J.APENERGY.2025.126698.

[20] Liu Y, Tang H, Chen Y, Wang D, Song C. Optimization of layout and diameter for distributed solar heating network with multi-source and multi-sink. Energy 2022;258:124788. https://doi.org/10.1016/J.ENERGY.2022.124788.

[21] Akbar D, Kilkiş B. Exergy-based optimization constraints for solar PVT panels and district energy systems with onboard green hydrogen production by solar prosumers. Energy Effic 2024;17:6. https://doi.org/10.1007/s12053-023-10184-8.

[22] Bogdanovics R, Zemitis J, Zajacs A, Borodinecs A. Small-scale district heating system as heat storage for decentralized solar thermal collectors during non-heating period. Energy 2024;298:131260. https://doi.org/10.1016/J.ENERGY.2024.131260.

[23] Lee M, Han C, Kwon S, Kim Y. Energy and cost savings through heat trading between two massive prosumers using solar and ground energy systems connected to district heating networks. Energy 2023;284:129347. https://doi.org/10.1016/J.ENERGY.2023.129347.

[24] Calise F, Cappiello FL, Dentice d'Accadia M, Petrakopoulou F, Vicidomini M. A solar-driven 5th generation district heating and cooling network with ground-source heat pumps: a thermo-economic analysis. Sustain Cities Soc 2021:103438. https://doi.org/10.1016/j.scs.2021.103438.

[25] Tang H, Liu Y, Chen Y, Wang D, Yuan X. Distributed solar heating system with busbar thermal reservoir network: Dynamic modeling and techno-economic analysis. Appl Therm Eng 2024;246:122987. https://doi.org/10.1016/J.APPLTHERMALENG.2024.122987.

[26] Frison L, Kollmar M, Oliva A, Bürger A, Diehl M. Model predictive control of bidirectional heat transfer in prosumer-based solar district heating networks. Appl Energy 2024;358:122617. https://doi.org/10.1016/J.APENERGY.2023.122617.

[27] Testasecca T, Catrini P, La Villetta M, Beccali M, Piacentino A. Energy assessment of thermal solar-powered district heating and cooling networks for a cluster of buildings in Mediterranean climate. Renew Energy 2025;251:123397. https://doi.org/10.1016/J.RENENE.2025.123397.

[28] Russo G, Olympios A V., Forzano C, Pandey C, Buonomano A, Palombo A, et al. A comprehensive techno-economic analysis of solar energy integration in low-temperature district heating and cooling systems. Renew Energy 2026;256:124017. https://doi.org/10.1016/J.RENENE.2025.124017.

[29] Zeng Q, Tian Z, Chen X, Li L, Ma L, Chen X, et al. Towards next generation zero carbon heating plants integrated with solar thermal/photovoltaic system and thermal storage. Energy 2025;336:138483. https://doi.org/10.1016/J.ENERGY.2025.138483.

[30] Zajacs A, Bogdanovičs R, Zeiza-Seleznova A, Valančius R, Zemītis J. Integration of decentralized solar collectors into a district heating system. Sustain Cities Soc 2022;83:103920. https://doi.org/10.1016/J.SCS.2022.103920.

[31] Pans MA, Claudio G, Eames PC. Transition pathways for a gas supplied district heating network to an ultra low carbon district heating network: A case study for Holywell Park,

Loughborough University. Renew Energy 2025;255:123841. https://doi.org/10.1016/j.renene.2025.123841.
[32] Somawanshi A, Kowli A. Scheduling Heat Pumps for Balancing Thermal Storage and Grid Export. Energy Informatics: First Nordic Energy Informatics Academy Conference, EIA Nordic 2025, Stockholm, Sweden, August 20–22, 2025, Proceedings, Part II, Berlin, Heidelberg: Springer-Verlag; 2025, p. 204–20. https://doi.org/10.1007/978-3-032-03098-6_14.
[33] Ahrens Kayayan V, Cabral D, Gustafsson M, Johari F. Multi-Energy Interplay in a Planned District Community with a Large Share of PV-Produced Electricity in a Nordic Climate. Buildings 2025;15. https://doi.org/10.3390/buildings15173112.
[34] Li L, Zhao J, Tian Z, Chen X, Jalilov D, Juraev T, et al. Synergistic deployment of electric heat pumps and pit thermal energy storage for renewable energy integration and heating decarbonization. Energy Build 2026;356. https://doi.org/10.1016/j.enbuild.2026.117079.
[35] Østergaard PA, Duic N, Noorollahi Y, Kalogirou S. Informing heating electrification and prosumer-based solutions toward decarbonisation targets via a multi-objective optimization in grid-connected PV systems in rural buildings. Energy 2025;330:136869. https://doi.org/10.1016/j.renene.2023.119377.
[36] Sornek K, Homa M, Frigura-Iliasa FM, Frigura-Iliasa M, Jankowski M, Papis-Frączek K, et al. Power-to-Heat and Seasonal Thermal Energy Storage: Pathways Toward a Low-Carbon Future for District Heating. Energies (Basel) 2025;18. https://doi.org/10.3390/en18215577.
[37] Dogkas G, Tsimpoukis A, Itskos G, del Castillo JC, Lozano I, Gustafsson O, et al. Analysis of a hybrid heating system with TRNSYS: district heating, heat pumps and photovoltaics in a multi-apartment building. Energy Build 2025;344:116011. https://doi.org/10.1016/j.enbuild.2025.116011.
[38] Calise F, Cappiello FL, Cimmino L, Cuomo FP, Vicidomini M. A 5th generation district heating cooling network integrated with a phase change material thermal energy storage: A dynamic thermoeconomic analysis. Appl Energy 2025;389:125688. https://doi.org/10.1016/j.apenergy.2025.125688.
[39] Ahrens Kayayan V, Cabral D, Israelsson K, Gustafsson M. Positive energy districts in Sweden: The impact from heat pumps, photovoltaic systems, and energy recovery from district heating return pipe. Energy Build 2025;334:115471. https://doi.org/10.1016/j.enbuild.2025.115471.
[40] Massulli AR, Rosa FC, Lo Basso G. Moving Towards Fourth-Generation District Heating as a Power-to-Heat Strategy: Techno-Economic Issues. Sustainability 2025;17. https://doi.org/10.3390/su17083675.
[41] Calise F, Liberato Cappiello F, Cimmino L, Dentice d'Accadia M, Vicidomini M. Optimal design of a 5th generation district heating and cooling network based on seawater heat pumps. Energy Convers Manag 2022;267:115912. https://doi.org/10.1016/j.enconman.2022.115912.
[42] Ochs F, Magni M, Dermentzis G. Integration of Heat Pumps in Buildings and District Heating Systems—Evaluation on a Building and Energy System Level. Energies (Basel) 2022;15. https://doi.org/10.3390/en15113889.
[43] Klein Sa, Beckman A, Mitchell W, Duffie A. TRNSYS 17-A TRansient SYstems Simulation program. Solar Energy Laboratory, University of Wisconsin, Madison 2011.
[44] Deru M, Field K, Studer D, Benne K, Griffith B, Torcellini P, et al. U.S. Department of Energy Commercial Reference Building Models of the National Building Stock. 2011.
[45] La Villetta M, Catrini P, Piacentino A. Dynamic simulation of a heat pump for building applications oriented to assess the potential for demand response and ancillary services supply. Energy Build 2025;344:116006. https://doi.org/10.1016/J.ENBUILD.2025.116006.

[46] UNI. UNI/TR 11552:2014 "Opaque envelope components of buildings - Thermo-physical parameters n.d.
[47] European Standards. EN 14511:2022-Air conditioners, liquid chilling packages and heat pumps for space heating and cooling and process chillers, with electrically driven compressors. 2022.
[48] Catrini P, La Villetta M, Kumar DM, Morale M, Piacentino A. Analysis of the operation of air-cooled chillers with variable-speed fans for advanced energy-saving-oriented control strategies. Appl Energy 2024;367:123393. https://doi.org/10.1016/J.APENERGY.2024.123393.
[49] IMST-Group Instituto de Ingeniería Energética Universidad Politécnica de Valencia. IMST-Art 2021.
[50] Blanco Castro J, Urchueguía JF, Corberán JM, Gonzálvez J. Optimized design of a heat exchanger for an air-to-water reversible heat pump working with propane (R290) as refrigerant: Modelling analysis and experimental observations. Appl Therm Eng 2005;25:2450–62. https://doi.org/10.1016/j.applthermaleng.2004.12.009.
[51] Pisano A, Martínez-Ballester S, Corberán JM, Mauro AW. Optimal design of a light commercial freezer through the analysis of the combined effects of capillary tube diameter and refrigerant charge on the performance. International Journal of Refrigeration 2015;52:1–10. https://doi.org/10.1016/j.ijrefrig.2014.12.023.
[52] Pitarch-Mocholi M, Navarro-Peris EE, Gonzalvez-Macia J, Corberan JM. Comparative analysis of two subcritical heat pump boosters using subcooling in order to increase the efficiency of systems with a high water temperature glide . 12th IEA Heat Pump Conference, Rotterdam : 2017.
[53] Corberán J-M, Martínez-Galván I, Gonzálvez-Maciá J, Martínez-Ballester S. Influence of the source and sink temperatures on the optimal refrigerant charge of a water-to-water heat pump. IIR 1st Workshop on Refrigerant Charge Reduction, France: 2009.
[54] Holmgren WF, Hansen CW, Mikofski MA. pvlib python: a python package for modeling solar energy systems. J Open Source Softw 2018;3:884. https://doi.org/10.21105/joss.00884.
[55] European Commission Joint Research Centre. Heat Pumps in the European Union. Luxembourg, 2025. https://publications.jrc.ec.europa.eu/repository/bitstream/JRC144191/JRC144191_01.pdf